CHAPTER 7 JOINT DEFORMATION AND COMPARISON WITH ANALYTICAL RESULTS

7.1 INTRODUCTION

To study the stress distribution and the deformation at the pipe joint, various attempts have been made (the Concrete pipe Association of Australia 1983, Milligan and Ripley 1989, Norris 1992, and Haslem 1996). For its simplicity, the Australian model is now widely used in practice. In this chapter, two analytical models, the Australian model and the flexible pipe model (Haslem 1996), are briefly reviewed in Section 7.2. The displacements at the joint from numerical model B in Chapter 5 are discussed in Section 7.3. The results from the numerical model C in Chapter 6 are described and compared with those from the Australian model and the flexible pipe model in Section 7.4. The conclusion is given in Section 7.5.

7.2 ANALYTICAL MODELS

Two analytical models, the Australian model and the flexible pipe model (Haslem 1996), are discussed in this section. In both models, the pipes adjacent to the joint are assumed to be under the edge loading condition, and shear stresses at the joint are ignored.

7.2.1 THE AUSTRALIAN MODEL

The Concrete Pipe Association of Australia (1983) published a theory of joint behaviour. In the Australian model, it is assumed that there exists a partial gap between the pipe and the packing material and the diametrical contact width is Z as shown in Figure 7.1. Moreover, it is assumed that the normal stress varies linearly from zero at the front of the gap to the

maximum stress σ_{max} at the pipe edge on the interface (see Figure 7.1) and that the stresses in the pipe and in the packing material have the same distribution pattern as that on the interface. The axial strain in the pipe and the packing material are linearly related to the normal stress at the joint. The analysis presented by the Concrete Pipe Association of Australia is summarised below.

The total load transferred at the pipe joint is obtained by integrating the normal stresses distributed over the joint (on the interface). As discussed above, the stresses are distributed over a contact width Z and the maximum stress σ_{max} is at the pipe edge ($x = R$). Figure 7.2 shows a diagram of the stress integration and the integration procedure is described as following. The cross length of the element at x in the figure is L_x:

$$L_x = 2\sqrt{R^2 - x^2} - 2\sqrt{r^2 - x^2} \qquad \text{when } |x| < |r|$$

$$L_x = 2\sqrt{R^2 - x^2} \qquad \text{when } |x| > |r| \qquad (7.2.1)$$

where R and r are the external radius and internal radius of the pipe. The stress intensity on this element is:

$$\sigma = \sigma_{min} + \sigma_m \ (x - H_1) \ / \ (R - H_1) \qquad (7.2.2)$$

where

$$\sigma_{min} = \max\left(0, \ \frac{(Z - 2R)\sigma_{max}}{Z}\right), \quad \sigma_m = \sigma_{max} - \sigma_{min}$$

$$H = R - Z, \quad H_1 = \max(H, \ -R) \qquad (7.2.3)$$

The total force transferred at the joint (P) is derived as follows:

$$P = \int_{H_1}^{R} \sigma L_x \, dx = P_0 + P_1 - P_2 \qquad (7.2.4)$$

where

$$P_0 = \pi (R^2 - r^2)\sigma_{min} \qquad (7.2.5)$$

$$P_1 = \int_{H_1}^{R} 2\sigma_m \left(\frac{x - H_1}{R - H_1}\right)\sqrt{R^2 - x^2}\, dx$$

$$= \frac{1}{R - H_1}\left[\frac{2}{3}(R^2 - H_1^2)^{\frac{3}{2}} + H_1^2\sqrt{R^2 - H_1^2} - H_1 R^2 \cos^{-1}\left(\frac{H_1}{R}\right)\right]\sigma_m \qquad (7.2.6)$$

$$P_2 = \int_{H_2}^{r} 2\sigma_m \left(\frac{x - H_1}{R - H_1}\right)\sqrt{r^2 - x^2}\,dx$$

$$= \frac{1}{R - H_1}\left[\frac{2}{3}(r^2 - H_2^{\,2})^{\frac{3}{2}} + H_1 H_2 \sqrt{r^2 - H_2^{\,2}} - H_1 r^2 \cos^{-1}\left(\frac{H_2}{r}\right)\right]\sigma_m \qquad (7.2.7)$$

where

$$H_2 = \text{sgn}(H)\,\min(|H|,\ r) \qquad (7.2.8)$$

Clearly, the maximum stress on the joint σ_{max} can be obtained by combining equation (7.2.1) to (7.2.8) when the contact width Z and the total transferred load P are known.

The total maximum compression deformation at the pipe edge (where σ_{max} is located) is derived as following:

$$\Delta a = \Delta a_p + \Delta L \qquad (7.2.9)$$

Where Δa is the total compression deformation, Δa_p is the deformation of the packing material and ΔL is the deformation of the two halves of the pipes adjacent to the joint. Assuming a linear relationship between the stress and strain, equation (7.2.9) becomes:

$$\Delta a = \frac{\sigma_{max}\, a}{E_p} + \frac{\sigma_{max}\, L}{E_c} \qquad (7.2.10)$$

where a is the thickness of the packer, L is the length of the pipe, E_p and E_c are the Young's modulus of the packing material and the concrete pipe. (In the original description of the Australian model, the possibility of different values of pipe thickness and wall thickness at joint was included. In the discussion in this project, the wall thickness at pipe joint is the same as the pipe thickness.)

From the Figure 7.1, the misalignment angle β can obtained from the total maximum compression deformation of the joint using the equation:

$$\tan\beta = \frac{\Delta a}{Z} \qquad (7.2.11)$$

Where Z is the diametrical contact width at the pipe joint.

7.2.2 HASLEM'S FLEXIBLE PIPE MODEL

To extend the Australian model to include tensile stresses, Haslem (1996) proposed a flexible pipe model. In this model, the stress distribution pattern at the pipe joint and the deformation pattern of the packing material are assumed to be the same as those in the Australian model. However, the concrete pipes are assumed to be under uniform pressure and bending moment due to the eccentric jacking load at the joint. The misalignment angle of the pipeline at the joint consists of the angular deflection angle of the compressed packing material and the sum of the angular deflections (due to the bending moment) of the two halves of the pipes adjacent to the joint. Furthermore, it is assumed that the ends of the pipes remain plane during bending and that the bending moment is constant along the length of the two pipe halves.

The additional analysis of bending of the concrete pipes in this model is summarised as below. With the stress distribution as shown in Figure 7.1, the bending moment about the axis y can be calculated using the diagram in Figure 7.2 as following:

$$M = \int_{H_1}^{R} \sigma L_x \, x \, dx = \sigma_m F_e \tag{7.2.12}$$

where:

$$F_e = \int_{H_1}^{R} 2x\left(\frac{x-H_1}{R-H_1}\right)\sqrt{R^2-x^2}\,dx - \int_{H_2}^{r} 2x\left(\frac{x-H_1}{R-H_1}\right)\sqrt{r^2-x^2}\,dx$$
$$- \frac{1}{R-H_1}\left[\frac{R^4}{4}\cos^{-1}\left(\frac{H_1}{R}\right) - \frac{H_1}{4}(2H_1^2-R^2)\sqrt{R^2-H_1^2} - \frac{2}{3}H_1(R^2-H_1^2)^{\frac{3}{2}}\right]$$
$$- \frac{1}{R-H_1}\left[\frac{r^4}{4}\cos^{-1}\left(\frac{H_2}{r}\right) - \frac{H_2}{4}(2H_2^2-r^2)\sqrt{r^2-H_2^2} - \frac{2}{3}H_1(r^2-H_2^2)^{\frac{3}{2}}\right] \tag{7.2.13}$$

The misalignment angle β is obtained from the angular deflection of the compressed packing material (β_p) and the sum of the angular deflections of the two halves of the pipes adjacent to the joint (β_c) is as follows:

$$\beta = \beta_p + 2\beta_c \tag{7.2.14}$$

where:

$$\beta_p = \frac{\Delta a_p}{Z} = \frac{\sigma_{max}\, a}{Z E_p} \tag{7.2.15}$$

$$\beta_c = \frac{M L}{2 E_c I_c} \tag{7.2.16}$$

Where L is the length of the pipe, $I_c = \frac{\pi}{4}(R^4 - r^4)$ is the second moment of area of the cross-section of the concrete pipe. Similar to the Australian model, there is a relationship between the misalignment angle β, the maximum joint stress σ_{max}, the total transferred load P and the contact width Z. For example, with a constant load P, β and σ_{max} are both functions of Z as shown by equation (7.2.4) to (7.2.16).

7.3 JOINT DEFORMATION OF NUMERICAL MODEL B

In Chapter 5, several analyses using numerical model B are described. The load distribution pattern at the pipe end under 'edge' loading in Chapter 5 (refer to Figure 5.2) is the same as that assumed in the analytical model shown in Figure 7.1. This section describes the compression deformations at the pipe end (the axial displacements at the pipe end along the line of r = 715mm) in numerical model B with interface elements between the pipe and the surrounding soil (refer to Figure 5.8 and Section 5.4 in Chapter 5). The results under the 'edge' loading are compared with those from the Australian model and Haslem's flexible pipe model.

The computed displacements in the z direction at the top pipe end (axial displacements w at the bottom end are in the opposite direction) under 'edge' loading in numerical model B and the analytical results, from the Australian model and Haslem's flexible pipe model, are shown in Figure 7.3. The numerical results show that the distributions of the displacements are non-linear over the pipe end, and that the distribution patterns of the displacement are

similar in the cases of typical soil and soft soil while with some deviations in the case of stiff soil. The maximum magnitudes of the displacements are located at the pipe edge as expected. In the region close to the pipe edge (x < -400mm), the displacements vary almost linearly; On the right side (x > 0mm), the displacements are small and positive with the typical and soft soil; while in the region of the edge of the applied load (x = - 220mm), the tangent angles of the displacement curves change rapidly possibly due to the local bending effects. The results from the Australian model shows a linear displacement distribution in the loaded region (x = -220mm), and there is no displacement in the non-loaded region since the stresses in the concrete pipe are zero in this region. The displacements from the flexible pipe model is linearly distributed over the pipe end.

From the figure, it is clear that the numerical results with typical soil and soft soil are close to the analytical data from the Australian model to some extent except in the region of the edge of the applied load (x = -220mm). The results from Haslem's flexible pipe model deviate from the numerical ones. A possible reason is that the concrete pipes in the flexible pipe model are assumed to sustain tensile stresses in the axial direction due to the bending moment. From the numerical analysis in this research, the tensile stresses under edge loading are localised in the region of the pipe joint and are mainly located in the hoop direction. From Figure 7.1 and 7.3, the Australian model shows that the distribution of the misalignment angle at the pipe joint due to the deformation of the concrete pipe is dependent on the part with higher compression displacements in the loaded region. The deflection angles at the pipe end from the numerical and the analytical models are given in Table 7.1.

Table 7.1 Deflection angle at pipe end under edge load (degree)

typical soil	soft soil	stiff soil	Australian model	Haslem (1996)
0.0502	0.0544	0.0370	0.0675	0.0198

From the table, it is clear that the deflection angle from the Australian model is slightly higher than that from the numerical model with typical and soft soil, and the deflection angle from the flexible pipe model is much smaller due to the assumption of tensile stresses in the concrete pipe as discussed above.

Figure 7.4 shows the displacements (w) in z direction at the top pipe end under 'diagonal' loading in numerical model B. From the figure, it is clear that with the typical and soft soil the deformations at the pipe end are much larger than those under 'edge' loading and are mainly due to the rigid body rotation of the pipe in the soil. The influence of the stiffness of the surrounding soil is significant. The total deflection angles and the rigid rotation angles with different soils derived from the displacements are given in Table 7.2. It should be pointed out that these deformations tend to reduce the original misalignment angle at the pipe joint (Norris 1992, Ripley 1989). This means that the load distribution at the pipe end would change significantly under the diagonal load due to the deformation of the concrete pipe with typical and soft soil (Ripley 1989). In practice, misalignment angles under 'diagonal' loading condition are usually found to be much smaller than those under 'edge' loading condition due to the large pipe deformation. Unfortunately, there is no analytical model for this aspect of pipe behaviour.

Table 7.2 Deflection angle at pipe end under diagonal load (degree)

	typical soil	soft soil	stiff soil
Total deflection angle	0.2521	2.116	0.0587
Rigid rotation angle	0.2080	2.071	0.0238

7.4 RESULTS OF NUMERICAL MODEL C

In this section, the results from numerical model C are discussed. The deformation of the bottom pipe (in fact, it is half a pipe as shown in Figure 6.2 in Chapter 6) is described in Section 7.4.1. Section 7.4.2 discusses the misalignment angles at the pipe joint. The maximum stress and the diametrical contact width at the joint from the numerical model C are compared with the results from the Australian model and the flexible pipe model (Haslem 1996) in Section 7.4.3.

7.4.1 DEFORMATION OF THE BOTTOM PIPE

The deformation of the bottom pipe (again along the line of r = 715mm), which is under the 'edge' loading condition (see Figure 6.2 in Chapter 6), is discussed first. The displacements in the axial direction at the top end of the bottom pipe (w) with low applied misalignment angle β=0.09° and different packing materials are shown in Figure 7.5. The figure shows that the displacements change linearly (or almost linearly) over the pipe end and have their maximum magnitudes at the pipe edge and that the packing material with higher shear modulus and higher Poisson's ratio has higher rate of change of displacement at the pipe end. However, the influence of the properties of the packing material is small. (It is also seen that the influence is not only due to the stiffness of the packing material $E_p = 2G_p(1+\mu_p)$ because the maximum compression displacement in the case of G_p = 300MPa, μ_p = 0.4 (E_p = 840MPa) is higher than that in the case of E_p = 900MPa, μ_p = -0.3 (E_p = 1260MPa).)

Figure 7.6 shows the displacements in the axial direction at the top end of the bottom pipe with high applied misalignment angle β=0.27°. From the figure, it is clear that the displacements vary non-linearly over the pipe end and have a similar distribution pattern to

that in numerical model B except that the loaded region is now on the right side (x > 100mm). The displacements are high and almost linearly distributed in the region of x > 200mm, and are small and positive in the region of the left end (x < -150mm). The tangent angles of the displacement curves change rapidly in the region of the gap front (refer to Section 6.4, and see Figure 6.11 and 6.15 in Chapter 6). The influence of the properties of the packing material is small and similar to that under small applied misalignment angle.

7.4.2 MISALIGNMENT ANGLES AT PIPE JOINT

The total deformation at the pipe joint consists of the deformation of the packing material and the deformations of the two halves of the pipes adjacent to the joint (that is, the axial displacement w at the middle length cross section A-A of the top pipe in Figure 7.7 less the deformation of the interface). The total deformations at the pipe joint under low applied angle $\beta=0.09^0$ are shown in Figure 7.7. From the figure, it is clear that similar to the deformations of the bottom pipe the total deformations at the joint are almost linearly distributed over the pipe joint in all cases. The total deformation is smaller with the packing material having higher shear modulus and higher Poisson's ratio. However, the influence of the properties of the packing material is small.

Figure 7.8 shows the total deformations at the pipe joint under the high applied misalignment angle $\beta=0.27^0$. From the figure, it is clear that the total deformations are non-linear over the joint, and to some extent have similar distributions pattern as those of the deformation of the bottom pipe. Again, the influence of the properties of the packing material is small.

As discussed in Section 7.3, the actual misalignment angle at the joint can be obtained from the total deformation in the high compression region (loaded region). In the numerical model C, the diametrical contact width Z varies with y across the pipe thickness (refer to

Section 6.3 in Chapter 6, and see Figure 6.11, 6.12, 6.15 and 6.16). For simplicity, the misalignment angles under different conditions are calculated from the total deformation in the region $x > 250$mm. (In the case of low applied misalignment angle, the computed actual misalignment angles are independent of the calculation region.) The computed misalignment angles ($\overline{\beta}$) are given in Table 7.3.

The applied misalignment angle used in the numerical analysis is calculated from the given displacement δ in the x direction at the upper end of the top pipe as discussed in Chapter 6:

$$tan\,\beta = \delta / L \qquad (7.4.1)$$

where L is the length of the pipe. However, the displacement in the x direction at the centre of the bottom end of the top pipe (δ_b) is not zero. So the actual applied misalignment angle is as follows:

$$tan\,\beta^* = (\delta - \delta_b) / L \qquad (7.4.2)$$

The actual applied misalignment angles derived from this equation are also given in Table 7.3 for comparison with the computed misalignment angles.

Table 7.3 Actual applied and computed misalignment angle (degree)

$\beta = 0.09^0$		$\beta = 0.27^0$		packer's properties	
β^*	$\overline{\beta}$	β^*	$\overline{\beta}$	μ_p	G_p (MPa)
0.0671	0.0662	0.2100	0.2061	0.1	300
0.0643	0.0646	0.2056	0.1971	0.4	300
0.0685	0.0687	0.2124	0.2123	-0.3	300
0.065	0.0643	0.2076	0.1982	0.1	900
0.0641	0.0637	0.2063	0.1951	0.4	900
0.0656	0.0649	0.2083	0.1998	-0.3	900

From the table, it is clear that the computed misalignment angles agree well with the actual applied ones and that the influence of the properties of the packing material is small.

7.4.3 MAXIMUM STRESS AND DIAMETRICAL CONTACT WIDTH AT PIPE JOINT

In this section, the maximum stress σ_{max} and the diametrical contact width Z at the pipe joint from numerical model C are compared with the results from the analytical models under the computed misalignment angle $\overline{\beta}$. From the numerical results in Chapter 6 (refer to Figures 6.4, 6.5, 6.8, 6.9, 6.11, 6.12, 6.15 and 6.16), it is known that the stresses are non-linearly distributed over the joint, and that the diametrical contact width Z varies with y across the pipe thickness. In comparison, the average value of Z is used, or the contact width Z is calculated by interpolating linearly the stresses to a zero point if there is no gap between the pipe and the packing material; and the maximum stress σ_{max} at the pipe edge (x = 715mm) is calculated from the average stresses at the centre of elements in the region of the pipe edge ($\theta < 6^0$) with a linear interpolation.

In the analytical models, the stresses are assumed linearly distributed at the joint as shown in Figure 7.1 and for a particular joint the diametrical contact width Z and the maximum joint stress σ_{max} can be obtained as a function of the misalignment angle β under a constant applied load P as discussed in Section 7.2. The comparison between the numerical results and the analytical data is given in Table 7.4 for various packing materials. The results are obtained under uniform pressure q = 10MPa at the upper end of the top pipe as shown in Figure 6.2 in Chapter 6.

From the table, it is clearly seen that under small misalignment angles ($\overline{\beta} < 0.07^0$), the numerical results and the results from both analytical models agree well in all cases. With high misalignment angles ($\overline{\beta} > 0.195^0$), the numerical results and the results from the Australian model agree well, while the flexible pipe model gives much smaller contact width Z and much higher maximum stress σ_{max} due to the assumption of tensile stresses in the pipe, as discussed in Section 7.3. This means that the Australian model provides a good

approximation for the diametrical contact width Z and the maximum normal stress σ_{max} on average when the misalignment angle of the pipe line is known. Bearing in mind that the normal stresses in the region of the pipe edge ($\theta < 6^0$) change a little in the case of $\mu_p = 0.4$ as shown in Chapter 6 (refer to Figures 6.4, 6.8, 6.11 and 6.15), the Australian model likely underestimates the normal stresses in this region at the pipe joint.

Table 7.4 Comparison between the numerical and analytical results

	Australian model		Haslem (1996)		Numerical model C			
$\overline{\beta}$	Z	σ_{max}	Z	σ_{max}	Z	σ_{max}	packer's properties	
(degree)	(mm)	(MPa)	(mm)	(MPa)	(mm)	(MPa)	μ_p	G_p (MPa)
0.0662	1435.0	19.48	1435.0	19.48	1438	19.48	0.1	300
0.0646	1428.5	20.02	1428.5	20.02	1417	20.25	0.4	300
0.0687	1453.8	17.74	1453.8	17.74	1476	18.99	-0.3	300
0.0643	1335.7	21.39	1327.3	21.51	1390	20.98	0.1	900
0.0637	1326.2	21.57	1315.5	21.71	1338	21.20	0.4	900
0.0649	1370.3	20.87	1368.4	21.01	1415	21.00	-0.3	900
0.2061	768.0	32.4	505.0	43.69	804	33.50	0.1	300
0.1971	761.6	32.59	464.8	46.45	739	34.48	0.4	300
0.2123	820.1	30.95	621.8	37.62	848	30.40	-0.3	300
0.1982	700.4	34.6	296.7	66.40	698	36.90	0.1	900
0.1951	696.8	34.71	267.4	72.75	659	36.34	0.4	900
0.1998	722.3	33.83	371.0	55.20	704	36.50	-0.3	900

Note: $\overline{\beta}$ is computed misalignment angle (Section 7.4.3)

7.5 CONCLUSION

After the discussion and result comparison above, a few conclusions are drawn as following:

(1) With a linear stress distribution at two pipe ends under the 'edge' loading condition, the deformation of the pipe is non-linear over the pipe end, that is, the deformation is neither bilinear as the Australian model predicts nor linear as the flexible pipe model predicts. However, the Australian model, in general, gives a somewhat close prediction to the numerical results.

(2) Under small misalignment angle ('edge' loading) especially when the normal stress covers the whole (or almost whole) pipe joint, the pipe deformation and the normal stress at the pipe joint are almost linearly distributed, and the two analytical models give very close predictions to the numerical results.

(3) With a high misalignment angle ('edge' loading), there is a big gap between the pipe and the packing material, and both the deformation and the normal stress are non-linear over the pipe joint. From the point of view of average values, the Australian model gives good approximations about the diametrical contact width Z and the maximum normal stress σ_{max} at the joint; while the prediction from the flexible pipe model is poor, especially with the stiff packing material. due to the assumption of tensile stresses in the axial direction within the pipe.

(4) Under the 'diagonal' loading condition, the displacements at the pipe ends are mainly due to the rigid body rotation of the pipe within the soil, and with typical and soft soil, the deflection angle is higher than that under 'edge' loading. Because the deflection angle in this case reduces the original misalignment angle at the joint, in practice the misalignment angle is usually found to be small under 'diagonal' loading.

(5) Neither analytical model considers shear stress at the joint, which plays an important role in the pipe's performance.

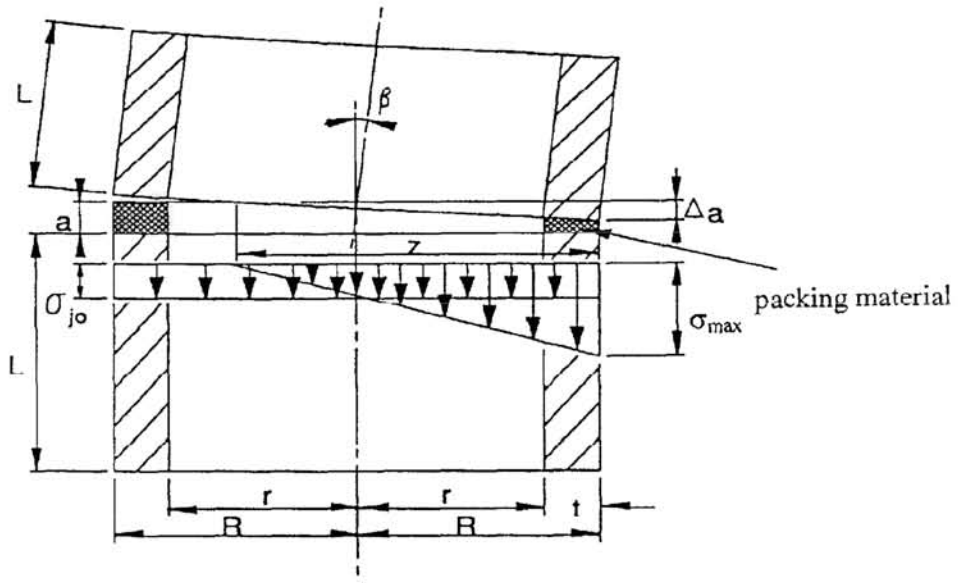


Figure 7.1 Australian joint stress distribution

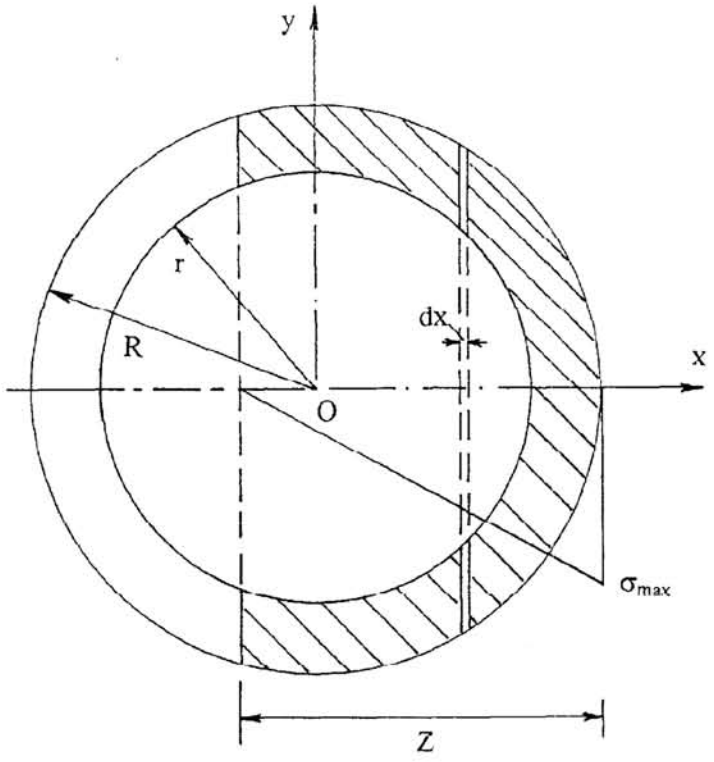


Figure 7.2 Integration diagram for joint stresses

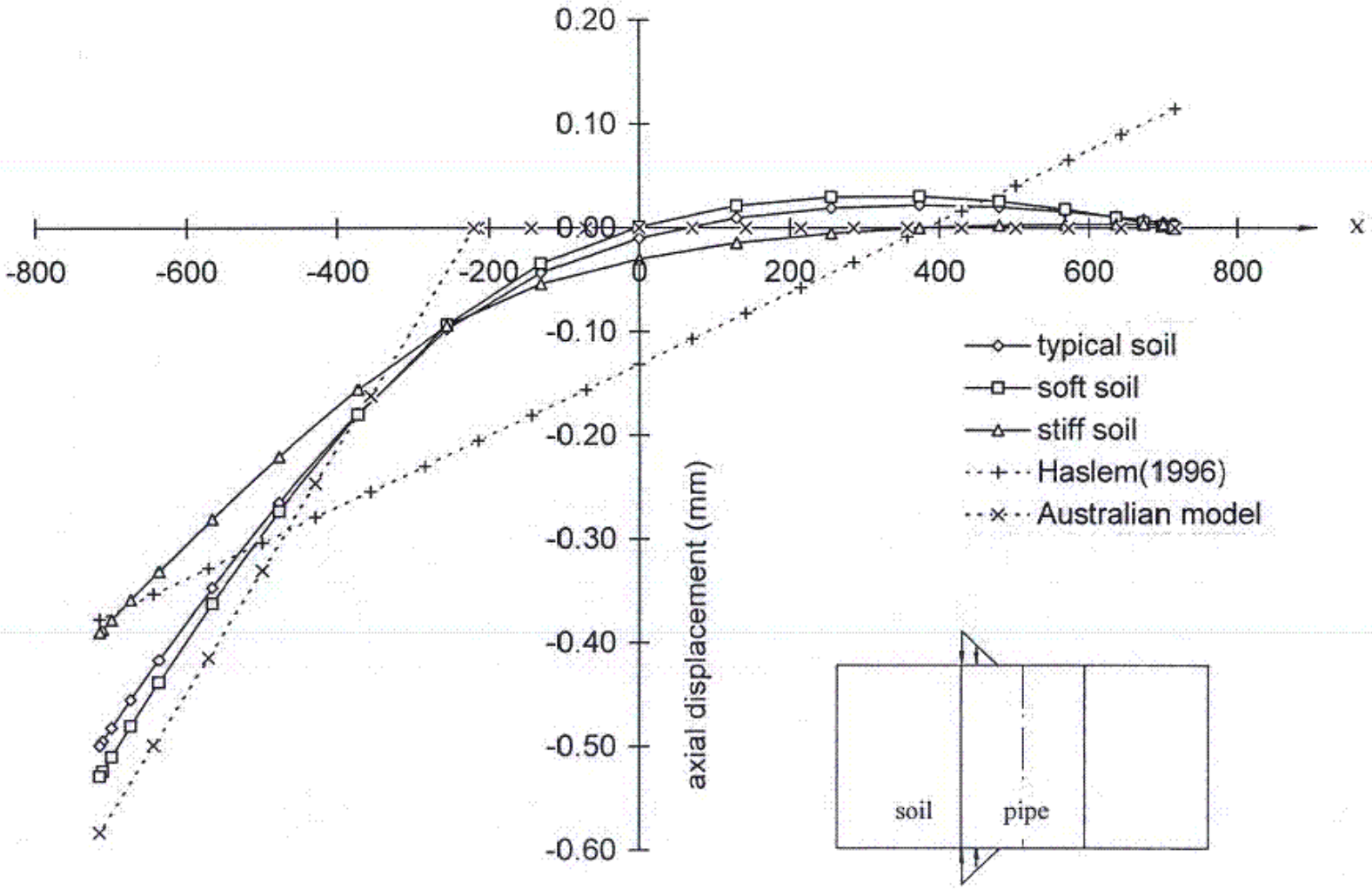


Figure 7.3 Compression displacement at the pipe end in numerical model B under edge loading

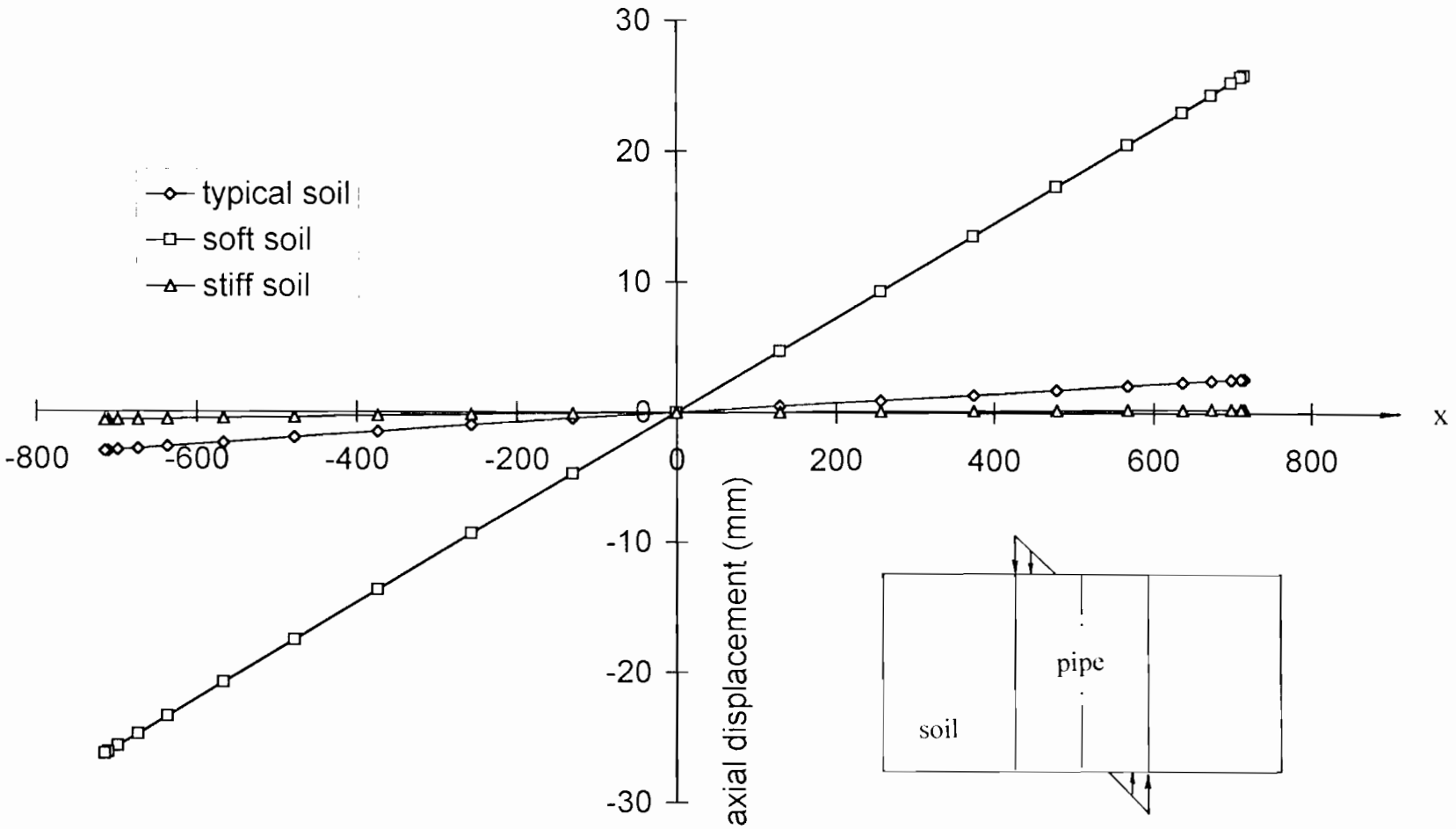


Figure 7.4 Compression displacement at the pipe end in numerical model B under diagonal loading

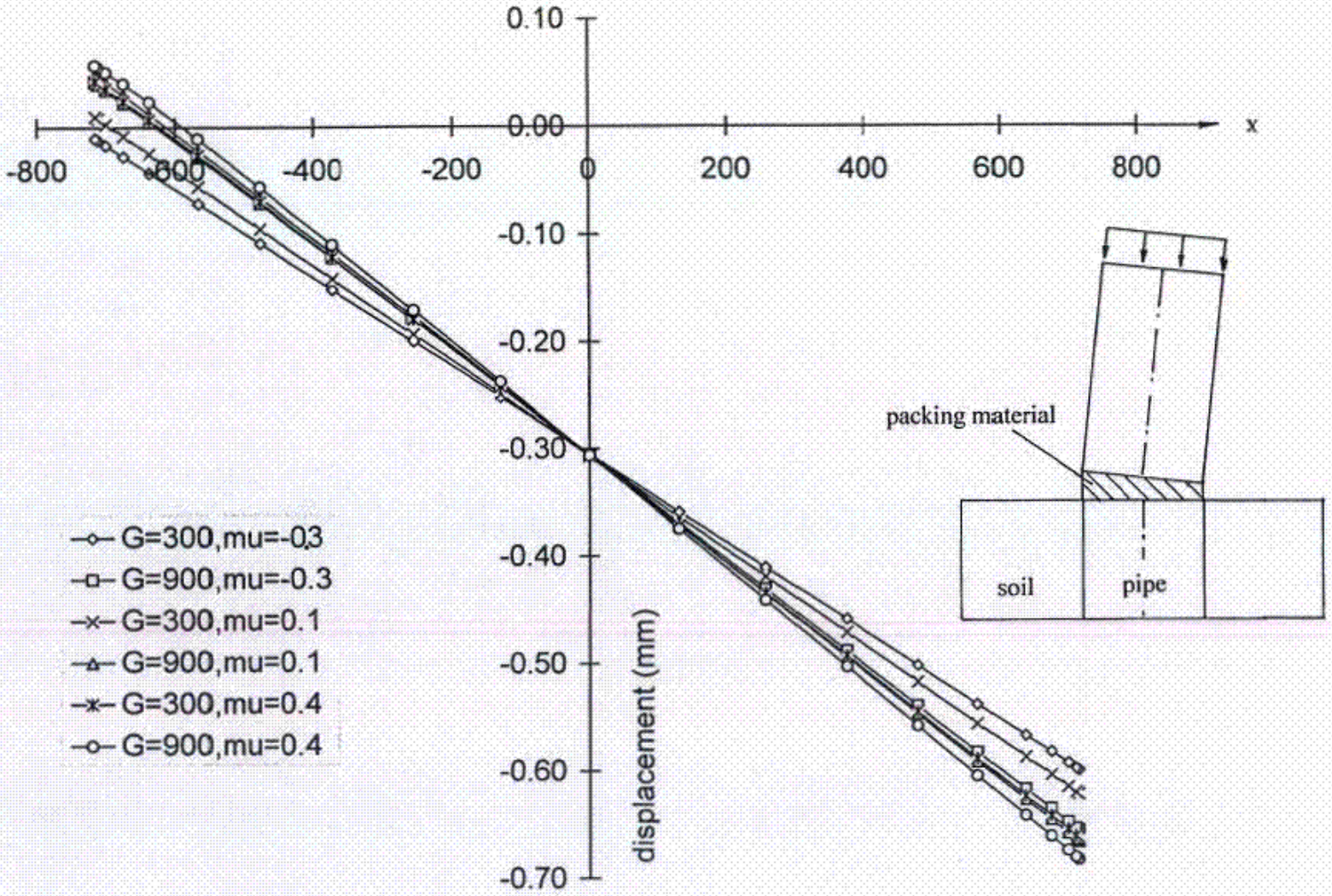


Figure 7.5 Compression displacement of the bottom pipe in numerical model C with $\beta=0.09^0$

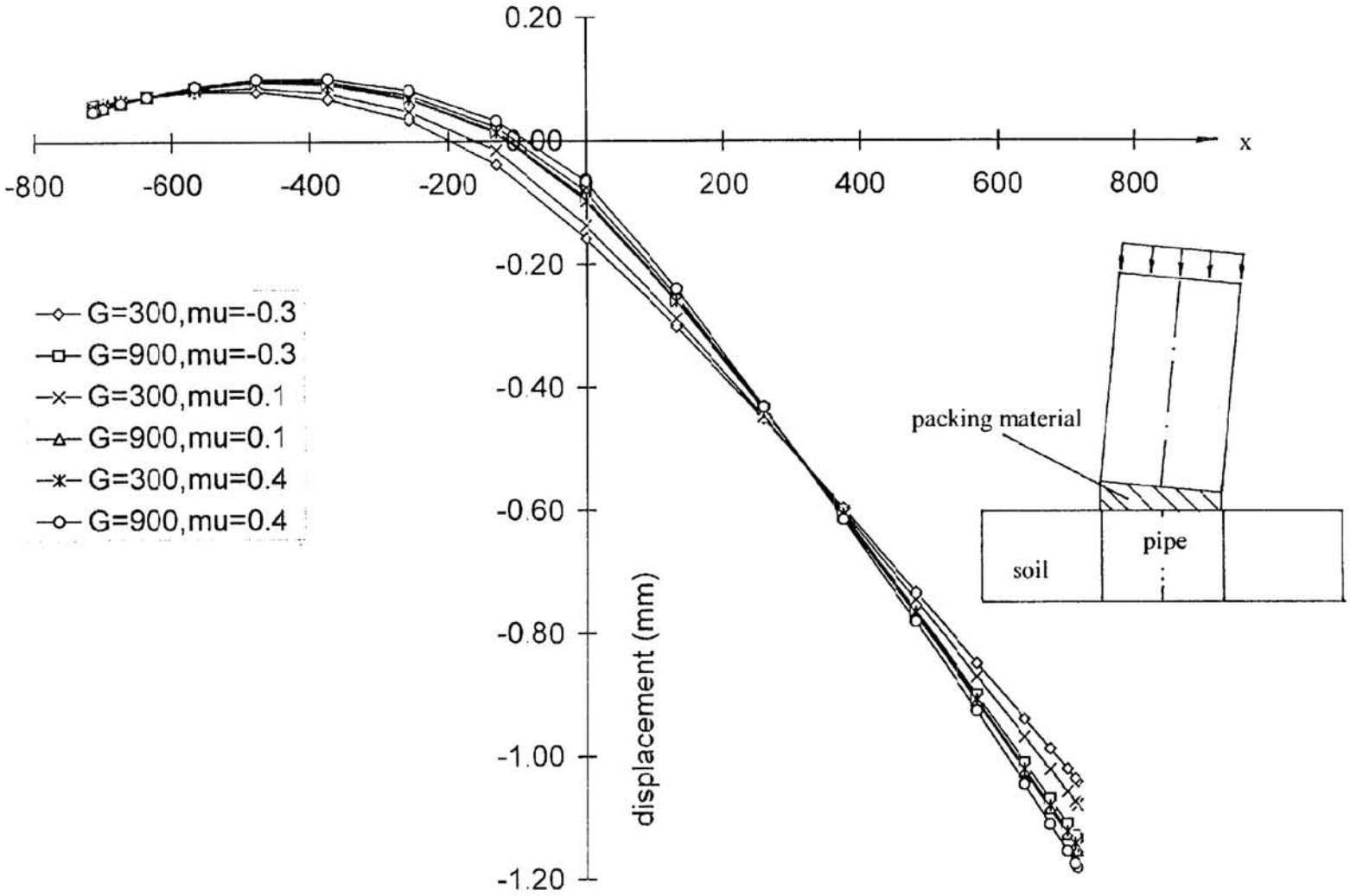


Figure 7.6 Compression displacement of the bottom pipe in numerical model C with $\beta=0.27^0$

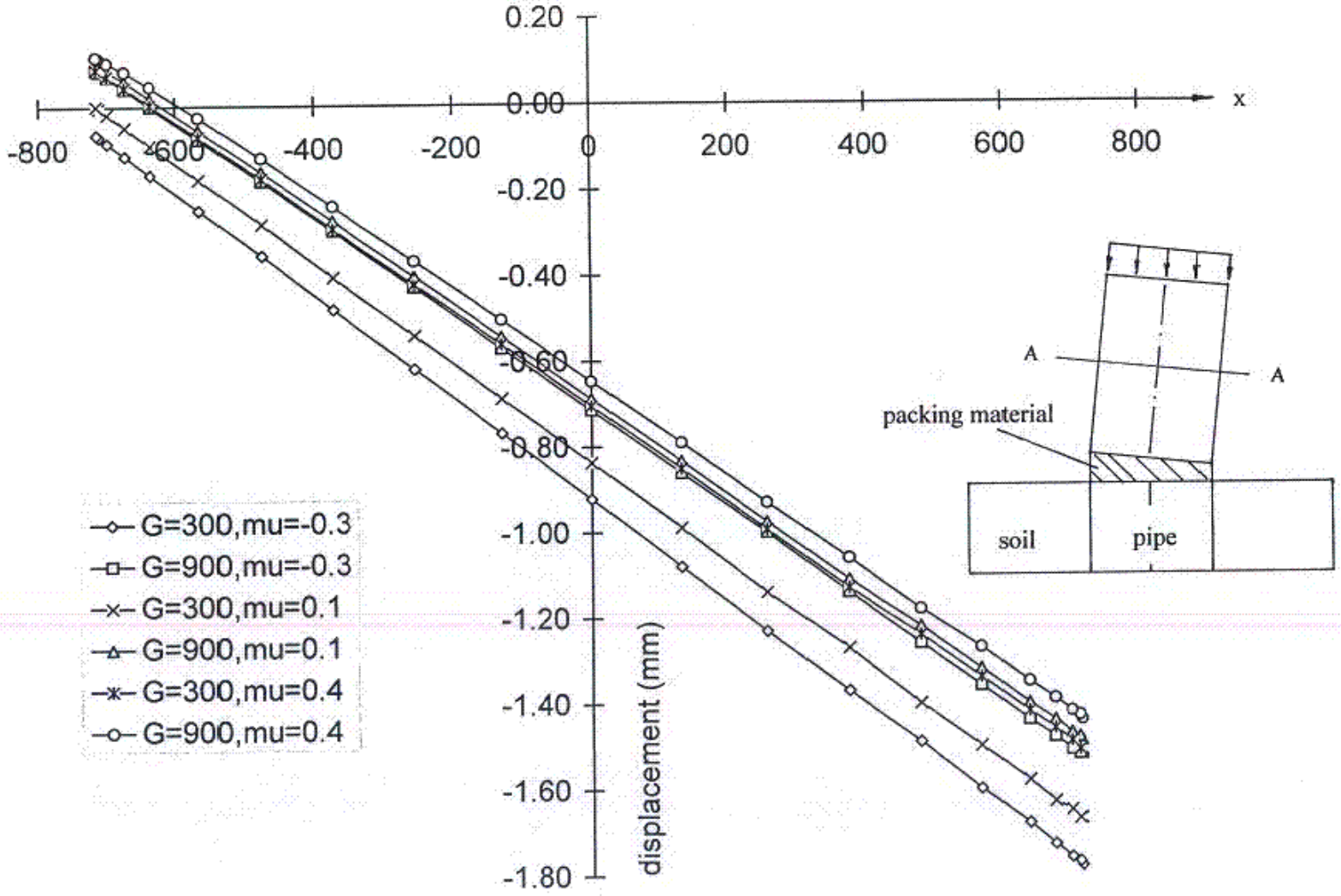


Figure 7.7 Total deformation at the joint in numerical model C with $\beta=0.09^0$

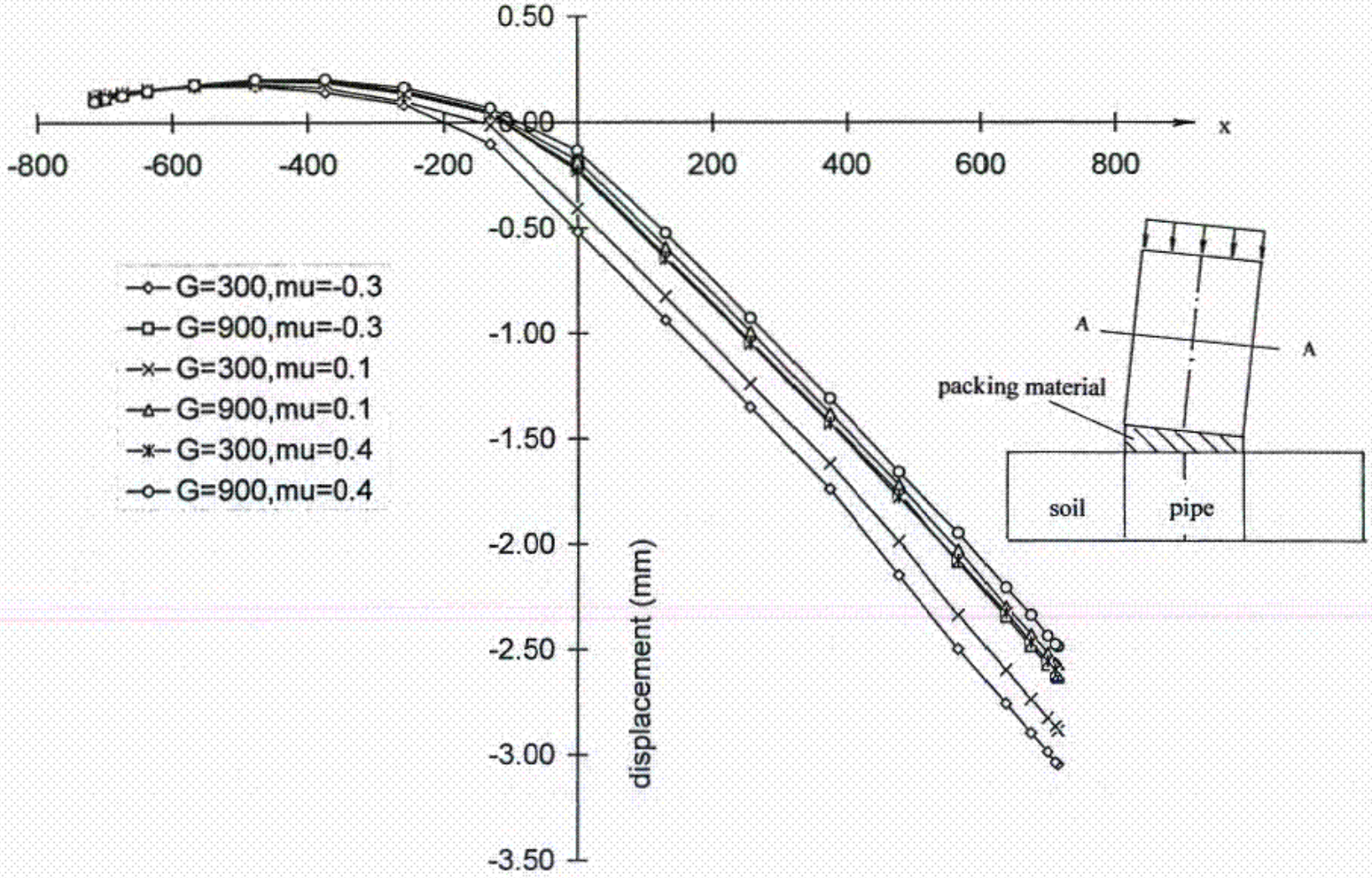


Figure 7.8 Total deformation at the joint in numerical model C with $\beta=0.27^0$